Effect of Alloy Composition on the Oxidation Behaviour and Cr Vaporisation of High-Cr Steels for SOFC Cathode Air Preheater

Zhang, Kun; Hong, Jong-Eun; Steinberger-Wilckens, Robert

Effect of Alloy Composition on the Oxidation Behaviour and Cr Vaporisation of High-Cr Steels for SOFC Cathode Air Preheater

K. Zhang[a], J. E. Hong[b], R. Steinberger-Wilckens[a]

[a] Fuel Cell Research Group, School of Chemical Engineering, University of Birmingham, B15 2TT, United Kingdom
[b] Fuel Cell Laboratory, Korea Institute of Energy Research, 152 Gajeong-ro, Yuseong-gu, Daejeon, 34129, Republic of Korea

We investigated the capability of aluminised and alumina-forming alloys to reduce the Cr vaporisation and increase the corrosion resistance by the growth and formation of alumina scale. The Cr evaporation tests have been performed for Inconel 625, AluChrom 318, SS309 and aluminised SS309 by applying a denuder technique at 850 °C with 6 L/min airflow and 3 vol% H_2O to simulate the cathode atmosphere in SOFC. Chemical analysis of the oxide scales formed was subsequently studied by XRD and SEM/EDX. Inconel 625 and uncoated SS309 exhibited relatively higher Cr evaporation due to a Cr-rich oxide layer, in comparison with other materials. The chromium evaporation of uncoated SS309 was dramatically decreased by aluminising. The experiments showed that Cr retention of the aluminised surface of SS309 is comparable to that of alumina-forming steel, AluChrom 318, over 168 hours. However, spallation of PVD applied alumina scales was detected for aluminised SS309 after 1000 hours oxidation.

Introduction

In solid oxide fuel cell (SOFC) systems, the Cathode Air Preheater (CAPH) functions as a heat exchanger, recovering heat from the exhaust gas to heat air close to the operating temperature (900 ˚C) before it enters the fuel cell. The higher the effectiveness of the heat exchanger, the more energy is recovered from the exhaust gas and thus, the higher the overall efficiency of the plant. As a result of the high operating temperature (900 ˚C) and severe environment within the cells, the ideal material for CAPH applications should be manufactured from special alloys that are structurally and chemically stable under both fuel and air atmosphere. The project HEATSTACK is looking into issues of CAPH in SOFC systems, including manufacturability, structural integrity, and chromium release. The current CAPH prototype employs an advanced Cr-containing alloy to offer improved oxidation resistance under isothermal and cyclic conditions and provide sufficient mechanical support. However, high temperature oxidation and Cr vaporisation are still critical issues that will have detrimental effects on SOFC stack. Volatilisation of hexavalent Cr such as CrO_3 and $Cr(OH)_2O_2$ will form over the Cr_2O_3 scale in oxidising environment at high temperature (1-3). A number of researchers have proven that $Cr(OH)_2O_2$ is the dominant Cr-containing volatiles under SOFC cathode environment (3-5). The evaporated Cr that leaves the surface eventually deposits onto and poisons the cathode, leading to significant performance degradation (6).

Foremost among alloys for CAPH application are aluminium-containing material, mainly because their excellent corrosion resistance is based on the protective alumina scales. Alumina-forming materials have been utilised for a wide range of applications such as catalyst supports in automotive application because of their high corrosion resistance and stability. Normally, the concentration of Cr inside alumina-forming alloy is around 20 wt.%. The added Cr boosts the formation of an external α-Al_2O_3 layer by reducing the ingress of oxygen into the alloy during high temperature exposure (7). However, the ductility of alumina-forming alloys is considered to be poor due to their high Al content (8). Another possible solution to the cathode-side chromate production is to form a protective alumina layer by surface aluminising. Aluminising enhances the oxidation resistance of alloys at high temperature without influencing the mechanical properties of the test materials in the core. The purpose of this study was to quantitatively measure the Cr species evaporated from Inconel 625, AluChrom 318, uncoated SS309, and aluminised SS309 by means of the denuder technique at the temperature of 850 ˚C. This research also determined if the corrosion resistance and Cr evaporation performance of SS309 can be improved by aluminising. In addition, the suitability of aluminised chromia-forming alloys and alumina-forming alloys for CAPH application concerning the reduction of Cr evaporation will be discussed.

Materials and Methods

Materials

Four commercial alloys were selected for this research. The samples were coupons of the Cr-containing alloy with the dimensions 15×15×0.3 mm^3. The alloy compositions for these materials in wt.% are shown in Table 1. One material, stainless steel 309 (SS309), was aluminised on both sides in order to compare the high temperature corrosion behaviour with uncoated SS309. The 1 μm aluminium film was coated by Teer Coating Ltd with a proprietary physical vapor deposition (PVD) process. All samples were exposed in an as-received status after being cleaned in acetone and ethanol using an ultrasonic bath.

TABLE I: The chemical compositions of the researched materials supplied by manufacturer.

(wt.%)	Fe	Cr	Mn	Al	Ni	Si	Nb	W	Co	others
AluChrom 318	Bal.	18.8	0.21	3.58	0.24	0.32	0.73	2.02	--	Hf 0.06; Y 0.07 Zr 0.03; Cu 0.03 C 0.01; N 0.01
Inconel 625	5.0	20-23	0.5	0.4	Bal.	0.5	4.15	-	1.0	Ti 0.4; Mo 8-10 P 0.015; S 0.015
SS309	Bal.	22-24	2.0	--	12-15	0.75	--	--	--	C 0.2; P 0.045 S 0.03

Exposures

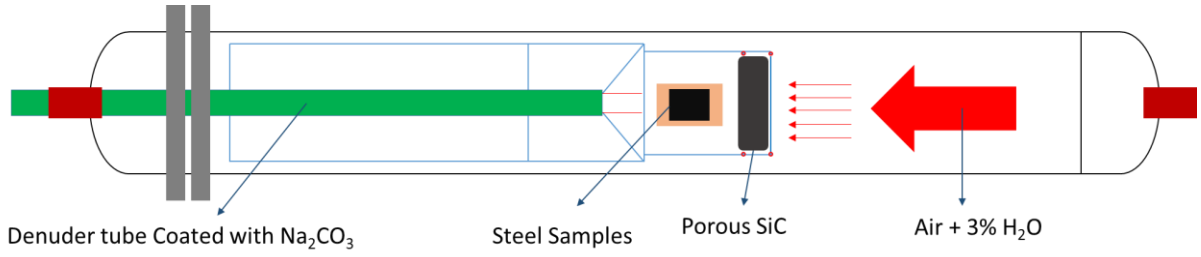

Figure 1.The schematic diagram of denuder technique.

For the Cr evaporation test, the volatile Cr species were measured by isothermally exposing three same samples of stainless steel using a denuder technique (9) in a tubular furnace at 850 °C (Figure 1). The tests were carried out in an atmosphere consisting of air that was humidified with 3 vol% of water to simulate an SOFC cathode environment. The air flow rate was controlled to 6000 ml/min which corresponds to a regime where the evaporation rate is flow independent (9). As shown in Figure 1, directly upstream of the samples, a porous SiC functioning as a flow restrictor was placed obtain a uniform flow pattern. Downstream of the samples, the gas steam was fed through the quartz glass denuder tube, which has an i.d. of 5 mm. The inner wall of the denuder tube is coated with Na_2CO_3 which is used for Cr collection. The Cr-containing gas ($CrO_2(OH)_2$) produced in the simulated SOFC environment reacts with the Na_2CO_3 to produce Na_2CrO_4 on the basis of Equation (1):

$$CrO_2(OH)_2\,(g) + Na_2CO_3\,(s) \rightarrow Na_2CrO_4\,(s) + H_2O\,(g) + CO_2\,(g) \qquad (1)$$

After collection, the inside wall of the denuder tube was subsequently washed with 10 ml distilled water. UV-vis spectrophotometer analysis applied to the obtained solutions offered quantification of the total amount of evaporated Cr species.
A high temperature oxidation test was additionally carried out by exposing different types of materials simultaneously at the same temperature and flow for a total time of 1000 hours. The difference between the high temperature oxidation test and the Cr evaporation test was that in the former case stainless steel samples were removed at increasing time intervals for gravimetric measurement and characterisation. For Cr collection, the denuder tubes were replaced without cooling down the furnace, allowing for uninterrupted measurement of Cr evaporation.

Characterisation

The gravimetric measurements were carried out using a Cubis Micro Balance (MSA2.7S0TRDM). The microstructure of the surface of non-exposed and exposed samples were studied by scanning electron microscopy/energy dispersive X-ray spectroscopy (SEM/EDX) (Tabletop Microscope TM3030, Hitachi-Hitec)

Results and Discussion

Mass Gain

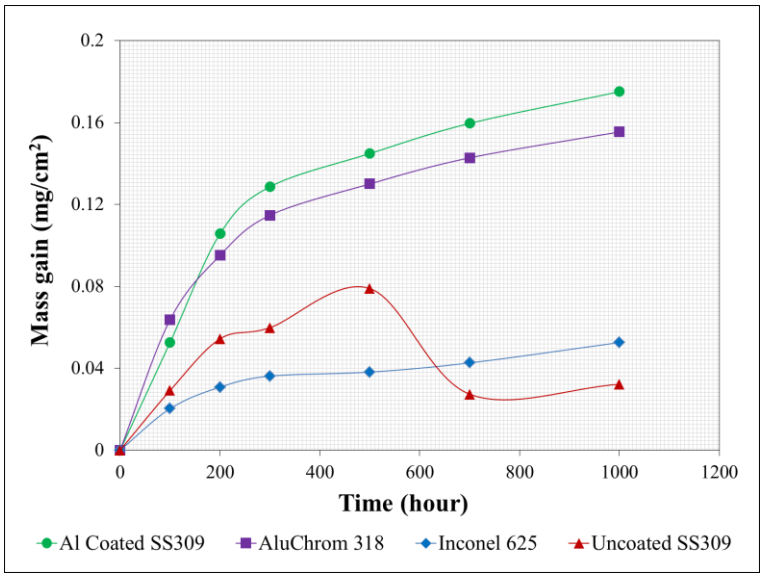

Figure 2. Discontinuous mass measurements for aluminised SS309, AluChrom 318, Inconel 625, and uncoated SS309 in 3 vol% H_2O humidified air at 850 ˚C.

Figure 2 shows the mass gain of the four materials, AluChrom 318, Inconel 625, uncoated SS309, and Al coated SS309, as a function of time. The samples were exposed at 850 ˚C with 6.0 L/min air + 3 vol% H_2O for 1000 hours. All the materials displayed parabolic net mass gain behaviour. Up to 500 hours, the uncoated SS309 substrate showed a mass gain of 0.079 mg/cm^2. However, the substrates appeared to then show a mass loss and started to suffer from severe spallation. It was observed that, after 500 hours, a large amount of black powder was detected on the sample holder of SS309, while the sample holders of other samples remained clean. The weight loss noted for uncoated SS309 is due to a combination of spallation of the oxide scale and Cr evaporation. This suggested that the oxide layer formed on the SS309 surface was unstable and not durable in simulated SOFC cathode environment. On the other hand, the aluminised SS309 showed a high and rapid mass gain without spallation. As can be seen, a mass gain of about 0.160 mg/cm^2 was recorded after 1000 hours, which is higher than that of the other Cr-containing steels. This is primarily because of the quick oxidation rate of Al in the early exposure, accompanied by the formation of an alumina layer. Nicolls *et al.* (10) reported that a higher oxidation rate was noticed for alloy with higher Al content at high temperature. The Ni based alloy, Inconel 625, showed a relatively low mass gain of about 0.043 mg/cm^2 after an exposure time of 1000 hours. AluChrom 318 with 3.58% Al content exhibited a mass gain of 0.143 mg/cm^2 which is slightly lower than aluminised SS309. Interestingly, all the Al-containing materials initially oxidized at a relatively faster rate than the alloys (uncoated SS309 and Inconel 625) without Al addition. This is because the protective Al-rich oxide layer that formed effectively protected the steel from high temperature Cr evaporation.

Chromium Evaporation

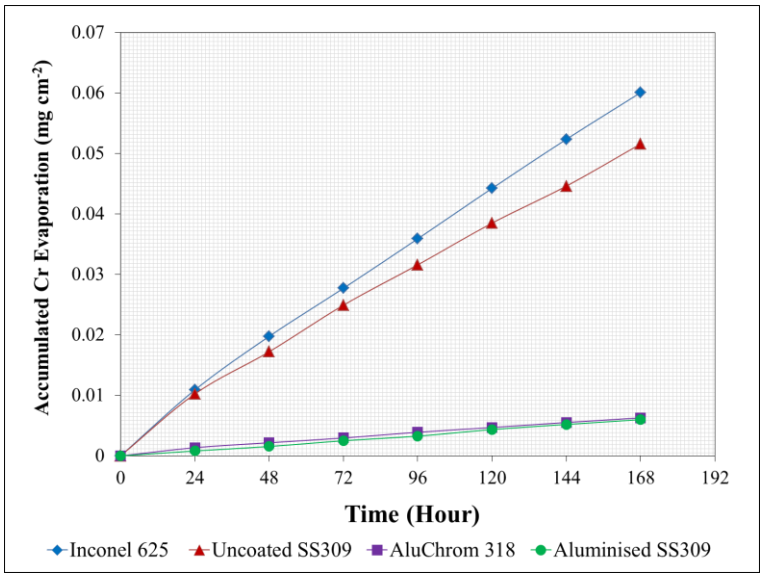

Figure 3. Accumulated Cr evaporation for Inconel 625, Uncoated SS309, AluChrom 318, and aluminised SS309 exposed to 3 vol% H_2O humidified air, 850 ˚C for 168 hours.

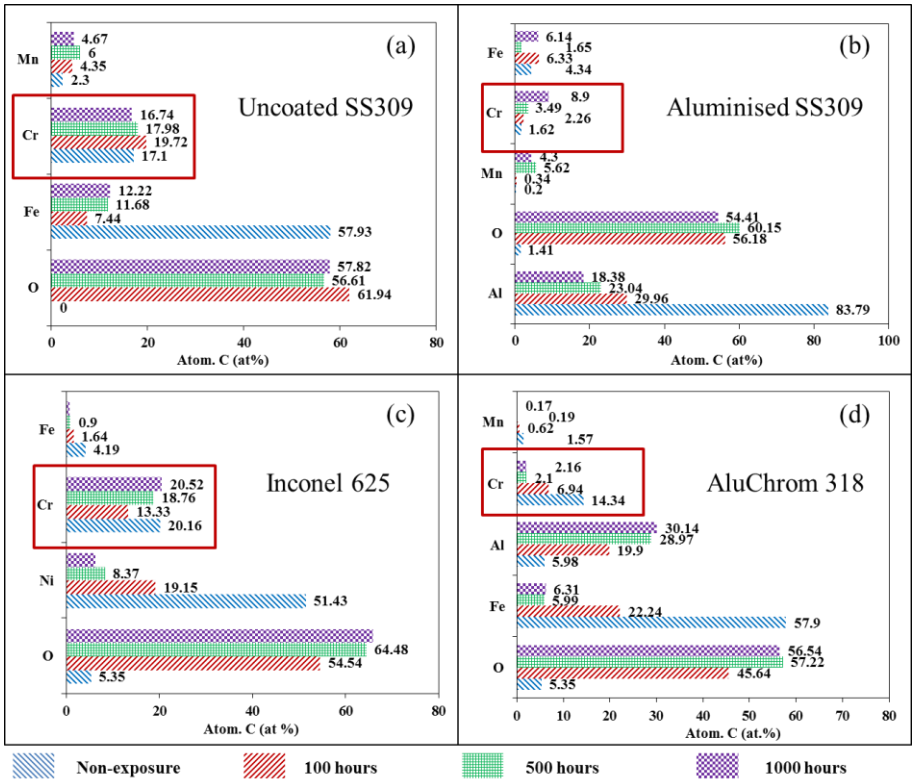

Figure 4. EDX elemental concentration of alloy surface exposure at 850 ˚C for 0, 100, 500 and 1000 hours: (a) uncoated SS309, (b) aluminised SS309, (c) Inconel 625, and (d) AluChrom 318.

The results of time resolved Cr evaporation tests performed on the investigated steels under isothermal conditions are presented in Figure 3. All the materials were measured for 168 hours. A comparison of the four commercial materials revealed that a significantly higher

amount of Cr evaporation was obtained from Inconel 625 (0.06 mg/cm^2), a factor of ten higher than AluChrom 318 and aluminised SS309. Furthermore, it can be seen from Figure 4(c) that the increase of Cr concentration from 13.33 at% to 20.52 at% indicates a thicker chromia scale is formed on the alloy surface, which is considered to be a detrimental factor for Cr leakage. Interestingly, Inconel also has the lowest value of mass gains, as shown in Figure 3. The lower mass gain of Inconel 625 could be both attributed to a lower oxidation rate and faster Cr evaporation rate (9). AluChrom 318 exhibited almost the lowest amount of Cr evaporation (0.006 mg/cm^2) of all the materials due to the relatively low level of Cr concentration (2.6 at%) (Figure 4(d)) after 1000 hours of exposure. Furthermore, the Cr concentration presented on the AluChrom 318 surface stayed constant from 500 hours onwards, indicating that alumina-forming steel could reduce high temperature Cr evaporation in the long term. It is worth noting that the Cr evaporation curve for AluChrom 318 in Figure 3 follows a more linear trend compared to other materials. The Cr evaporation rate for the aluminised SS309 (0.006 mg/cm^2) is approximate one order of magnitude lower than that for the uncoated SS309 (0.051 mg/cm^2). The measured Cr evaporation of aluminised SS309 is comparable to that of AluChrom 318, as can be seen from Figure 3. It should be noted that the Cr evaporation rate of aluminised SS309 showed a slightly increased trend after 72 hours, and the Cr concentration dramatically increased to 8.9 at% (Figure 4(b)) after 1000 hours of exposure. This phenomenon was caused by spallation of the oxide scale and will be discussed later in the SEM section. The extremely low amount of Cr evaporation for AluChrom 318 and SS309 is accredited to the presence of the aluminum content, which significantly reduces the Cr evaporation from the alloy surface due to the formation of a dense and continuous Al_2O_3-rich scale (8, 11). The rapid oxidation of the aluminium to an outer Al_2O_3 –rich layer acts as chromium barrier which inhibits the outward diffusion of the Cr element during high temperature exposure; thus a significantly reduced Cr evaporation is observed. This gives evidence of the excellent Cr retention ability of alumina.

Microstructural Investigation

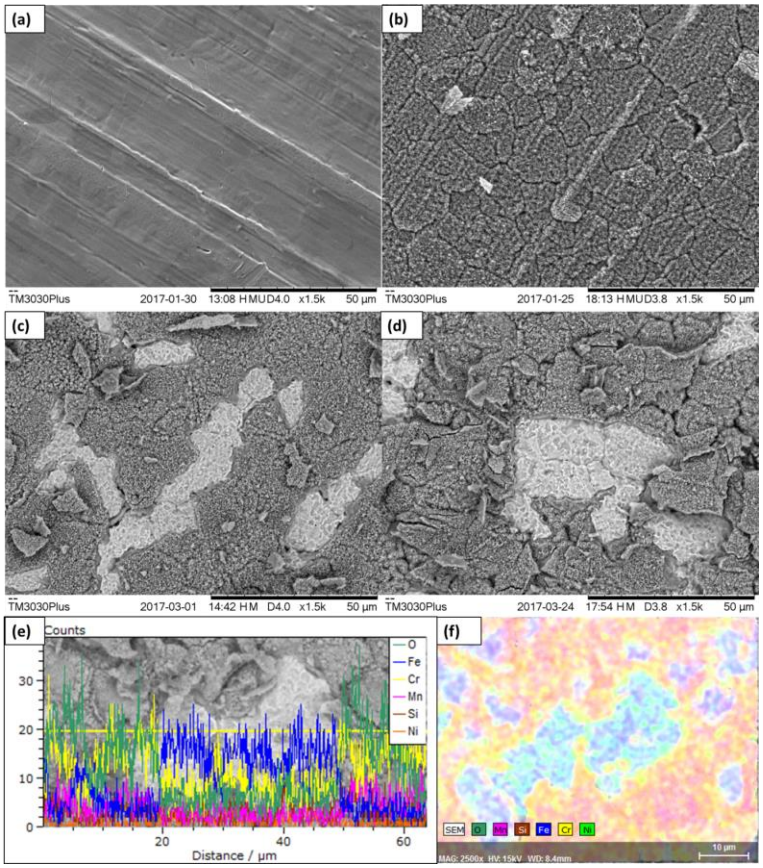

Figure 5. SEM images of uncoated SS309 exposed at 850 ˚C for: (a) 0 hour, (b) 100 hours, (c) 500 hours, and (d) 1000 hours. EDX line scan (e) and EDX maps (f) from the steel through the oxide scale of the uncoated SS309 after 1000 hours of exposure at 850 ˚C.

Figure 5(a-d) shows the SEM images of SS309 exposed for 0, 100, 500 and 1000 hours at 850 ˚C. The grain boundaries can be clearly detected on the unexposed SS309 surface (Figure 5(a)). After 100 hours exposure, a cracked oxide layer was formed on the SS309 surface, as shown in Figure 5(b). EDX results revealed that the surface oxides were composed of a top layer of Cr-Mn spinel with traces of Fe. However, spallation of this layer was detected at various positions after 500 hours of exposure (Figure 5(c)). The small oxide pieces with non-homogeneous size delaminated from the cracked surface, and scattered all around the alloy surface. An EDX study (Figure 5(e-f)) pointed out that the exposed layer beneath the Cr-Mn spinel contained very high amounts of Fe and Ni with traces of Cr. This phenomenon became even worse with exposure times increasing to 1000 hours. The Fe-rich region increased in size and more Cr-Mn spinel scales were spalled off compared to 500 hours of exposure, as can be seen from Figure 5(d). Results from Grolig et al. (12) are in line with the observation of this study, they also noticed a large amount of spallation on the uncoated AISI 441 exposed at the same conditions as this study for 500 hours. Note that the growth of Laves phases could be dramatically promoted by the addition of niobium content inside the alloy (13). Grolig *et al*. (12) stated that the number of Laves phases was not sufficient to bind silica and inhibit subscale silica formation at high temperature, which is generally suggested to induce spallation. In this study, SS309 is categorised as high Si steel (0.75 wt.%) that contains no niobium. Therefore, the Cr-Mn oxide scale formed on SS309 surface showed relatively bad adhesion properties.

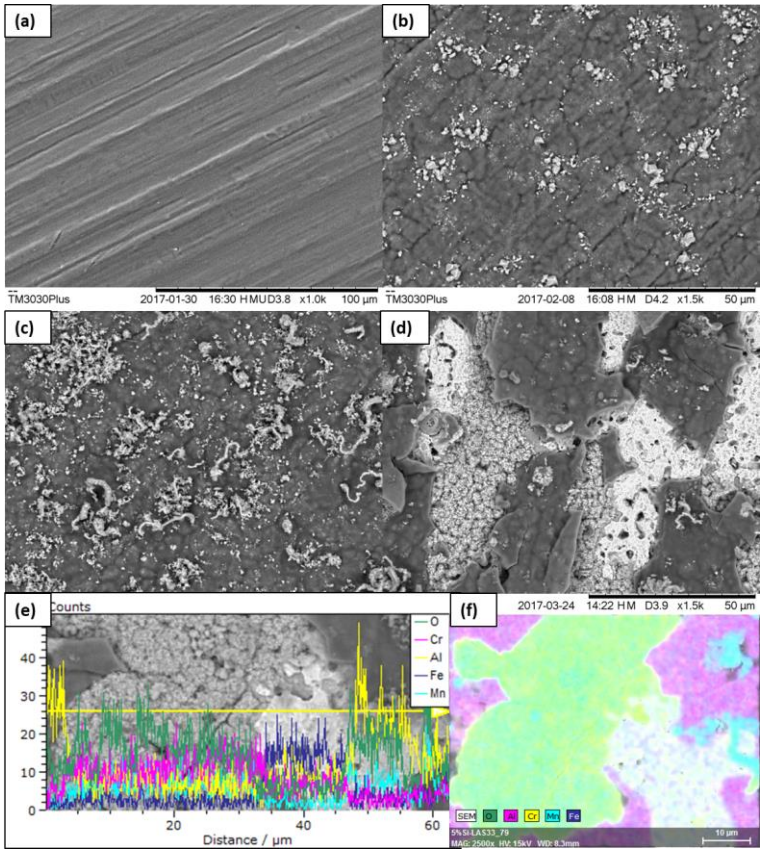

Figure 6. SEM images of aluminised SS309 exposed at 850 ˚C for: (a) 0 hour, (b) 100 hours, (c) 500 hours, and (d) 1000 hours. EDX line scan (e) and EDX maps (f) from the steel through the oxide scale of the aluminized SS309 after 1000 hours of exposure at 850 ˚C.

SEM images of aluminised SS309 samples exposed for 0, 100, 500, and 1000 hours are shown in Figure 6(a-d). As can be seen in Figure 6(a), the grain boundary is no longer visible on the aluminised SS309 surface compared with uncoated SS309, which has now been completely covered by the 1 µm aluminum coating. After 100 hours exposure, the aluminised SS309 surface appeared to be covered with alumina oxide scales with small and polygonal crystallite randomly distributed on the surface (Figure 6(b)). EDX results revealed that the major ingredient of the formed oxide scales consists of Al_2O_3 (Figure 6(e-f)). The composition of the polygonal crystallite is primarily composed of Mn_2O_3. After 500 hours of exposure, the surface of the Al_2O_3-rich oxide scale (Figure 6(c)) appeared to have a texture similar to the sample with 100 hours of exposure. No sign of spallation was detected for aluminised SS309 after 500 hours of exposure. The most surprising finding of this material was that a large amount of spallation was observed after 1000 hours of exposure. As can be seen from Figure 6(d), a large part Al_2O_3-rich oxide scale peeled off from the alloy surface, and Cr-Mn oxide scales and Fe-rich regions were exposed (Figure 6(f)). As mentioned above, the formation of a silica layer at the metal/oxide interface is often considered as the most relevant mechanism for oxide spallation on this type of material. EDX analysis showed that the concentration of Si on the aluminised SS309 surface presented an increasing trend from 0 at.% to 1.39 at%. Thus, it can be inferred that the great mass of Si was bound by Laves phases but a small proportion of Si diffused outward, to the oxide/metal interface, leading to spallation of oxide scales (12). This is also the reason that the high Cr concentration of 8.9 at% was found for aluminised SS309 after 1000 hours exposure (Figure 4(b)). As

mentioned above, an increased trend of Cr evaporation rate was noticed for aluminised SS309 after 72 hours. This is attributed to the spallation of Al_2O_3 scale, leading to the exposure of the Cr-rich oxide layer.

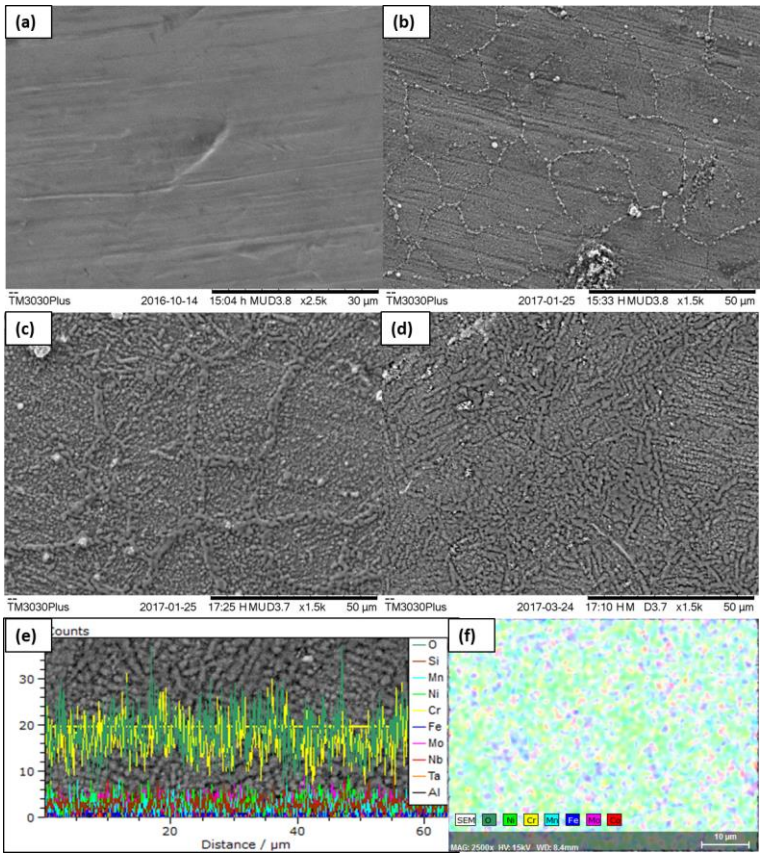

Figure 7. SEM images of Inconel 625 exposed at 850 ˚C for: (a) 0 hour, (b) 100 hours, (c) 500 hours, and (d) 1000 hours. EDX line scan (e) and EDX maps (f) from the steel through the oxide scale of the Inconel 625 after 1000 hours of exposure at 850 ˚C.

Figure 7(a-d) presents SEM images of Inconel 625 exposed at 850 °C for 0, 100, 500, and 1000 hours. The sample surface exposed for 100 hours exhibited a rougher and more porous surface with linear texture, in comparison with the non-exposed sample. The upward growth of oxide nodules along the grain boundaries was observed on the surface, and the growth path of oxide granules appeared to have a hexagon of shape, as can be seen from Figure 7(b). The visible cracks and gaps observed in the grain boundaries would be caused by the outmigration of cations from the alloy to the scale (14, 15). Ecer *et al.* (15) observed Cr depletion zones with voids inside the alloy, and the voids on the alloy grain boundaries were partially filled with Cr_2O_3. In this research, EDX analysis performed on the oxide granules revealed that their formation was mainly constituted by Cr and O elements, illustrating that the transport of Cr by grain boundaries could be the main reason for Cr evaporation. After 500 hours exposure, apart from the grain boundaries, it was observed that more oxide grains also grew from the porous surface and the whole surface became coarse and rough. In addition, an increasing number of Cr_2O_3 nodules grew upwards from the grain boundaries and aggregated into long strips with the exposure time increasing. Thus, Cr_2O_3 in the shape of long strips covered the whole alloy surface after 1000 hours of exposure, as shown in Figure 7(d). For uncoated alloys, one of the significant factors to offer high temperature oxidation resistance is the morphology of the spinel-containing scale (14). EDX line analysis (Figure 7(e)) taken

from the alloy surface indicated the oxide scale formed on the surface after 1000 hours exposure mainly consisted of Cr_2O_3. However, Mn was not detected on the oxide scales. Thus, it can be confirmed that the top oxide scales with a large amount of Cr would not protect the steel effectively. This phenomenon could also explain the largest quantity of Cr evaporation from Inconel 625 among the four materials, which also confirms the evaluation from gravimetric measurements (Figure 2).

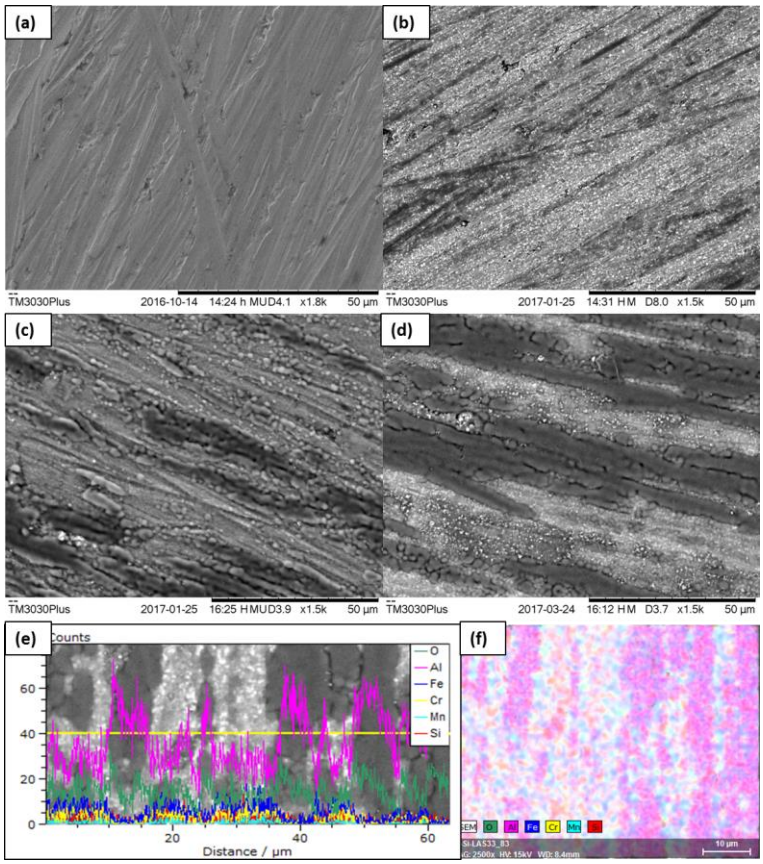

Figure 8. SEM images of AluChrom 318 exposed at 850 ˚C for: (a) 0 hour, (b) 100 hours, (c) 500 hours, and (d) 1000 hours. EDX line scan (e) and EDX maps (f) from the steel through the oxide scale of the AluChrom 318 after 1000 hours of exposure at 850 ˚C.

The surface morphology of AluChrom 318 exposed at 850 ˚C for 0, 100, 500, and 1000 hours is shown in Figure 8(a-d). The non-exposed sample (Figure 8(a)) had an uneven surface with lots of sharp scratches. After the high temperature oxidation for 100 hours, a relatively smooth and dense oxide film was observed with a large amount of light dots randomly distributed on the surface. As shown in Figure 4(d), the concentration of Al dramatically increased from 5.98 at% to 19.9 at%, while the concentration of Fe decreased from 57.9 at% to 22.24 at%. However, the Fe content still accounts for the most massive element on the alloy surface after 100 hours exposure. Thus, it can be inferred that the light dots presented on the alloy surface (Figure 8(e)) are Fe_2O_3. The surface of AluChrom 318 with the exposure time of 500 hours appeared to be partially covered with buckled oxide with dark grey color (Figure 8(c)). It is noteworthy that the buckled oxide scales became even large after 1000 hours exposure, while the light dots (Fe_2O_3) appeared to be reduced and covered by the buckled oxides. EDX results (Figure 8(e-f)) showed that buckled oxide contained Al and O with a small amount of Mn, indicating that a dense surface scale of α-Al_2O_3 had formed (8, 10). In addition, it can be noticed that the intensity of Al in the non-

buckled region is lower than that in the buckled region, which means that the non-buckled region is covered with a relatively thinner alumina scales. According to literature, the formation and growth of a alumina top layer is dependent on the outward flux of Al via grain boundaries (8, 16). It should be noticed that Fe_2O_3 and Cr_2O_3 were produced in the initial stage of oxidation on the surface of the alumina-forming alloy prior to the dense Al_2O_3-rich scale forming (7, 17, 18). The transient oxides (Fe_2O_3 and Cr_2O_3) are replaced by an Al_2O_3-rich scale. It is suggested that the Cr_2O_3 crystal serves as nucleation site for α-Al_2O_3 (7). The initially high Cr concentration in the oxide scale thus drops significantly in high temperature oxidation (17, 19). As mentioned above, the smallest proportion of Cr (2.16 at%) was detected by EDX for AluChrom 318 (Figure 4(d)). The additions of reactive elements such as Zr and Hf inside AluChrom 318 tend to cause micro porosity of the alumina scale. This could be a diffusion path for Cr to grow from the alloy to the oxide surface. After 500 hours oxidation, the gradient of Cr concentration flattens, as indicated by the EDX elemental concentration (Figure 4(d)). This reduction and low level of Cr concentration can be explained by the decrease of alumina scale thickening rate with increasing time.

Conclusions

The measurement of Cr evaporation from different alloys by a denuder technique exhibited that the amount of Cr evaporated from alumina-forming steel or aluminised steel is approximately one order of magnitude lower than that from pure chromia-forming steels. Although the Cr vaporisation level of aluminised SS309 is similar to that of AluChrom 318 for 168 hours, the Cr retention of AluChrom 318 was confirmed to be better than that of aluminized SS309 in the long term due to the spallation of Al_2O_3 scale on the aluminised SS309 surface.

Acknowledgements

This work was funded by European Union's Seventh Framework Program for the Fuel Cells and Hydrogen Joint Technology (FCH-JU) Initiative under grant agreement No. 700564. The authors would like to acknowledge the support of our collaborators in the HEATSTACK project.

References

1. H. C. Graham and H. H. Davis, *J.Am. Ceram. Soc*, **54**, 89 (1971).
2. K. Hilpert, D. Das, M. Miller, D. Peck and R. Weiss, *J. Electrochem.Soc*, **143**, 3642 (1996).
3. E. J. Opila, D. L. Myers, N. S. Jacobson, I. M. B. Nielsen, D. F. Johnson, J. K. Olminsky and M. D. Allendorf, *J. Phys. Chem. A*, **111**, 1971 (2007).
4. B. B. Ebbinghaus, *Combust. Flame.*, **93**, 119 (1993).
5. C. Gindorf, L. Singheiser and K. Hilpert, *J. Phys. Chem. Solid*, **66**, 384 (2005).
6. S. P. Jiang and X. Chen, *Int. J. Hydrogen Energy*, **39**, 505 (2014).
7. M. W. Brumm and H. J. Grabke, *Corros. Sci*, **33**, 1677 (1992).
8. M. Stanislowski, E. Wessel, T. Markus, L. Singheiser and W. Quadakkers, *Solid State Ionics*, **179**, 2406 (2008).
9. J. Froitzheim, H. Ravash, E. Larsson, L. G. Johansson and J. E. Svensson, *J. Electrochem.Soc.*, **157**, B1295 (2010).
10. J. R. Nicholls, M. J. Bennett, N. J. Simms, H. Hattendorf, D. Britton, A. J. Smith, W. J. Quadakkers, D. Naumenko, V. Kochubey, R. Fordham, R. Bachorczyk and D. Goossens, in

Novel Approaches to Improving High Temperature Corrosion Resistance, p. 129, Woodhead Publishing (2008).
11. Y.-S. Chou, J. W. Stevenson and P. Singh, *J. Power Sources*, **185**, 1001 (2008).
12. J. G. Grolig, J. Froitzheim and J. E. Svensson, *J. Power Sources*, **248**, 1007 (2014).
13. Y.-T. Chiu and C.-K. Lin, *J. Power Sources.*, **198**, 149 (2012).
14. Z. Chen, L. Wang, F. Li, K. C. Chou and Z. Sun, *Int. J. Hydrogen Energy*, **39**, 10303 (2014).
15. G. M. Ecer, R. B. Singh and G. H. Meier, *Oxid.Met.*, **18**, 55 (1982).
16. H. Falk-Windisch, J. E. Svensson and J. Froitzheim, *J. Power Sources*, **287**, 25 (2015).
17. W. J. Quadakkers, A. Elschner, W. Speier and H. Nickel, *Appl.Surf. Sci.*, **52**, 271 (1991).
18. J. Jedliński, A. Glazkov, M. Konopka, G. Borchardt, E. Tscherkasova, M. Bronfin and M. Nocuń, *Appl.Surf. Sci.*, **103**, 205 (1996).
19. W. J. Quadakkers, A. Elschner, H. Holzbrecher, K. Schmidt, W. Speier and H. Nickel, *Microchim. Acta*, **107**, 197 (1992).